Science and Technology Indonesia
e-ISSN:2580-4391 *p*-ISSN:2580-4405
Vol. 9, No. 2, April 2024

Research Paper

Modification of Indonesian Kaolinite-Based Silica Coarse (SC) for RNA Extraction Method of SARS-CoV-2

Marchia Marthalena Marintan[1], Fithriyah Sjatha[2], Dita Arifa Nurani[1,3], Yuni Krisyuningsih Krisnandi[1,3]*, Sariman Sariman[4]

[1]*Department of Chemistry, Faculty of Mathematics and Natural Sciences, Universitas Indonesia, Depok, 10430, Indonesia*
[2]*Department of Microbiology, Faculty of Medicine, Universitas Indonesia, Jakarta, 10320, Indonesia*
[3]*Solid Inorganic Framework Laboratory, Department of Chemistry, Faculty of Mathematics and Natural Sciences, Universitas Indonesia, Depok, 10430, Indonesia*
[4]*Research Center for Mining Technology, National Research and Innovation Agency (BRIN), Tanjung Bintang, 35361, Indonesia*
***Corresponding author**: yuni.krisnandi@sci.ui.ac.id

Abstract
One of the strategies to overcome the COVID-19 disease is through rapid diagnostic tests using the Reverse-Transcriptase Polymerase Chain Reaction (RT-PCR) test. The RT-PCR test is a detection and quantification test of nucleic acids, initiated by the pre-analytical step of purification of the nucleic acids. Purification of nucleic acid requires silica-based materials as a solid phase-extraction matrix or column. Herein, Silica Coarse (SC) in the form of suspension and powder columns; was prepared from natural Indonesian Kaolinite as an alternative extraction column to binding RNA of SARS-CoV-2. The RNA binding and releasing ability in SC was enhanced with the support of chaotropic agents in the form of Na^+ and Guanidium$^+$ as charged-balancing cations, embedded in the silicate layer inside the kaolinite framework. SC, which has been supported with Na^+ and Guanidium$^+$ respectively, then studied its physicochemical characteristics using FTIR spectroscopy, X-ray diffraction technique, scanning electron microscopy, and BET surface area and pore size measurement. This work shows that the modified SC suspension column could extract RNA of SARS-CoV-2 that amplified better in the RT-PCR test than SC powder columns, with the initial Ct value of all the SARS-CoV-2 specimens in the range < 20.

Keywords
SARS-CoV, Silica Matrix, Kaolinite, RNA Extraction Methods

Received: 26 October 2023, Accepted: 25 February 2024
https://doi.org/10.26554/sti.2024.9.2.325-335

1. INTRODUCTION

Since being discovered in December 2019 in the city of Wuhan, China; the novel coronavirus, better known as Severe Acute Respiratory Syndrome Coronavirus-2 (SARS-CoV-2), has spread tremendously and developed into the Coronavirus disease 2019 (COVID-19). The WHO states, that since April 10th, 2022, the number of COVID-19 confirmed cases has reached over 496 million people and over 6 million deaths have been reported. However, the SARS-CoV-2 virus can quickly spread through human-to-human interactions, so preventive and therapeutic strategies are needed to reduce the quick transmission of SARS-CoV-2 and prevent new clusters of COVID-19-positive cases (Lau and Chan, 2015). One of the strategies to control the COVID-19 disease is through diagnostic tests, including rapid antigen tests and RT-PCR tests (Ladha et al., 2020). Both of those tests take swab specimens from mucus in the nose and throat. Antigen rapid tests could process specimens relatively fast, but it easily led to false-positivity results (Sheridan, 2020). The RT-PCR test has the advantage of detecting human pathogens (Yoo et al., 2023; Ding et al., 2024) in this case, SARS-CoV-2, in real-time through fluorescence intensity changes in a closed tube that will avoid amplification manipulation and false results (Huang et al., 2011). RT-PCR test also has high reproducibility, analytical quantifications of nucleic acids, and is easy to use (Gibson, 2006). All of those advantages made RT-PCR the "gold standard"; or the standard diagnostic test of SARS-CoV-2 that is applied worldwide (Teymouri et al., 2021).

The basic principle of the RT-PCR test is similar to traditional PCR, using denatured target nucleic acids for amplification during thermal cycling. The only difference is the fluorometric probes in RT-PCR are used to bind target sequences of nucleic acid during the annealing phase of PCR (Shen, 2019). This step demands RNA that has already been purified without protein, lipid, and other contaminants to give accurate results. Thus, the swab specimens must undergo a pre-analytical step first, known as the step of isolation or extraction of nucleic acids. Nucleic acid extraction methods are classified into two, organic and inorganic methods (Song et al., 2024; Valiant et al., 2024).

The organic method uses phenol-chloroform for the extraction, but at this time the organic method is quite abandoned because of its toxic chemicals and labor-intensive (Farkas and Holland, 2009). Thus, the inorganic method which is principally based on Solid-Phase Extraction (SPE) analysis has become the main choice nowadays. According to SPE concepts, then the mobile phase is purified nucleic acids and the stationary phase could be silica matrices, glass particles, magnetic beads, or cellulose matrices. Among the stationary phases; silica matrices or silica columns are the most popular due to the ability to purify nucleic acids with high quality, low costs, reproducible, and low interferences in PCR amplification (Ali et al., 2017; Rimola et al., 2013). Some of the silica columns used for nucleic acid extraction consisted of silica thin layers with pore distributions <0.3 nm (Lee et al., 2011). The presence of chaotropic agents is an important support for the SiO_2 column, according to native conditions from the nucleic acid structure which is covered by a hydrated shell composed of water molecules. In the form of ions, chaotropic agents will damage the ordered structure of hydrated shells so that the nucleic acids will bind strongly on the silica column and release the nucleic acids (Katevatis et al., 2017; Zhang and Cremer, 2006). Chaotropic ions are also able to reduce the stability of proteins so they can denature RNAse enzymes, protein metabolites, and other contaminants that will affect the purity of nucleic acids. Further destruction of the hydrated shells will decrease the hydrophobic effect on nucleic acids so the nucleic acids will be easily released with an aqueous buffer and purified nucleic acids will be obtained (Wicky et al., 2017).

The preparation method of Silica Coarse (SC) as an extraction column for nucleic acids was initiated by Boom et al. (1990). That prior method was modified in this work by using natural Indonesian kaolinite as a silica source for its method. Kaolinite ($Al_2Si_2O_5(OH)_4$) is a natural aluminosilicate source classified as phyllosilicates with a 1:1 type structure. It consists of stacked aluminosilicate layers, one tetrahedral silica layer (T) fused to one octahedral alumina sheet (O), connected by H_2O interstitials. In the amorphous form, kaolinite often contains impurities such as metal oxides and organic matter (Frost et al., 2000; Loganathan et al., 2017). As a natural mineral source; kaolinite is mostly used as a raw component for functional materials such as catalysts, biological functional material, and also for adsorption studies (Gunawan et al., 2020; Baham and Sposito, 1994). Kaolinite has amphoteric sites on its basal and edge faces, (Gupta and Miller, 2010) the charge of amphoteric sites could be either net positive or net negative charged due to the amount of proton adsorbed on the layer of kaolinite (Chen et al., 2017; Tombácz and Szekeres, 2006. In this work, intercalation and modification of the amphoteric sites of kaolinite were reported, using chaotropic agent, Na^+ and Guanidium$^+$ ions, to develop net positive charged on the amphoteric sites so it will be bounded with phosphate groups from the nucleotide chain of SARS-CoV-2 which tend to be negatively charged. Indonesian kaolinite-based silica extracted from pre-treatment stages (Abdullah et al., 2020) will go through the SC preparation method and be modified through dispersion into 2 M CH_3COONa and 5 M GuSCN solutions; obtained SC-Na^+ and SC-Gu^+, respectively. SC-Na^+ and Gu^+ in the form of suspension pellets and powder are then used as a binding column for the RNA Extraction method of SARS-CoV-2. These are expected to be an initial formula for further fabrication of silica columns as a component in the RT-PCR diagnostic test kit. The result suggests that modified SC (suspension Column) has tremendous potential in the RNA extraction of SARS Cov-2 since the three RT-PCR signals FAM, VIC, and Cy5 can be detected from sample

2. EXPERIMENTAL SECTION

2.1 Materials and Instruments

The Indonesian kaolinite was provided by PT Aneka Kaolin Utama, Bangka Belitung, Indonesia. Hydrochloric acid, hydrogen peroxide 30%, ethanol, and sodium acetate were purchased from Merck (Germany). Guanidine thiocyanate was obtained from Sigma-Aldrich (United States). RNA from clinical specimens of the SARS-CoV-2 virus was provided by the Department of Clinical Microbiology, Faculty of Medicine, Universitas Indonesia. The viral nucleic acid extraction kit used in the RNA extraction method was purchased from QIAGEN (Germany). Characterizations of SC and its derivatives were carried by FTIR Alpha-Bruker for vibrational spectrum analysis, PANalytical XPert PRO 2318 diffractometer for XRD analysis, PANalytical Epsilon 1 for XRF analysis, and SEM-JEOL JSM-6510LA for SEM analysis. For analysis of surface area and pore size distribution was carried out with Quantachrom-Evo Surface Area and Pore-Analyzer instrument.

2.2 Pre-treatment of Indonesian Kaolinite

The pre-treatment of Indonesian kaolinite was carried out based on the previous study Saragi et al. (2019). Indonesian natural kaolinite was sieved to a size of ≤100 μm and then physically activated, purified, and thermally activated into metakaolin. Physical activation was performed by dispersing the kaolinite with distilled water (1:3 w/v) under vigorous stirring for 3 h at room temperature, then drying at 110 °C for 24 h. Purification of activated kaolinite was conducted by mixing it with sodium acetate solution adjusted to pH 5 and a mixture of 30% hydrogen peroxide: dithionite-citrate-bicarbonate (1:10 v/v). Afterward, the purified kaolinite was then subjected to a thermally activated process into metakaolin through calcination at 800-1000 °C. Silica extraction was performed by dissolving metakaolin in aquaregia solutions (HCl: HNO_3 with ratio of 3:1 (v/v)) under reflux for 4 h at 100 °C. Extracted silica then was washed until free from any content of acid and dried at 105 °C for 24 h.

2.3 Preparation of Silica Coarse (SC)

The preparation of Silica Coarse (SC) was referred to a study by Boom et al. (1990). Silica extracted from metakaolin is then prepared into Silica Coarse (SC). Before doing the SC preparation; all glassware, apparatus, and Teflon-autoclave should

be sterilized first with RNAse away solutions (ratio compositions of ethanol: HCl 0.0001 ppm (1:1 v/v)) to prevent any inhibition activities from RNAse denaturant (Toni et al., 2018). The extracted silica was dispersed into 50 mL of distilled water and precipitated for 24 h at room temperature. The remaining filtrate was separated, then the silica was dispersed again to 50 mL of distilled water and precipitated for 5 hours. The remaining 44 mL of filtrate was disposed and 600 μL of HCl was added to the precipitated silica. The precipitated silica was then transferred to a Teflon-lined stainless-steel autoclave (100 mL) and heated at 121 °C for 20 min. This process resulting the suspension of Silica Coarse (SC) then later modified with chaotropic agents, CH_3COONa and GuSCN.

2.4 Modification of Silica Coarse with CH_3COONa (Na^+-SC) and GuSCN (Gu^+-SC)

The preparation of modified SC with chaotropic agents, sodium acetate and guanidine thiocyanate, was done as follows: first typically 10 g kaolinite-based SC was dispersed into 300 mL of 2 M CH_3COONa and stirred for 6 h at room temperature. The resulting suspension was then left for 1 h to collect the SC precipitate, then was re-dispersed in 300 mL CH_3COONa 2 M and stirred vigorously for another 6 h. The suspension then left to stand for 24 h at room temperature so that the precipitated SC completely settled down and easily being decantated to obtain Na^+-SC. Half portion of the collected Na^+-SC from this process was used to form suspension columns and the other half was air-dried to form powder columns. The dried form of Na^+-SC was then calcined at 450 °C for 2 h. The calcination temperature is selected based on TGA characterization data (Supplementary Information, S1).

The Gu^+-SC was prepared from 10 g dried SC that was calcined at 450 °C and dispersed into 100 mL 5 M GuSCN. The suspension was then stirred for 4 h under vigorous stirring, left to stand for 24 h, and decanted to obtain Gu^+-SC precipitate. The precipitate was then autoclaved at 121 °C for 20 min to obtain Gu^+-SC in the form of suspension columns, while some part was subsequently dried at 100 °C to obtain Gu+-SC in the form of powder columns.

2.5 Ribonucleic acids (RNA) Extraction Method of SARS-CoV-2

The Ribonucleic acids (RNA) sample used in this extraction method was RNA of SARS-CoV-2; which came from the results of the RT-PCR test conducted at Clinical Microbiology Laboratory, Faculty of Medicine, Universitas Indonesia. All of the buffer solutions used in this method were commercial buffer solutions from QIAGEN-QIAMP® Viral RNA Extraction Kit, with modified kit instructions. Beforehand, the silica column was rinsed with washing buffer, to condition its column so that the chaotropic agents could be bound to the silica surface and weaken the amino acid interactions from remaining contaminant proteins inside the inactive RNA samples. The extraction tube was then centrifuged at 12,000 rpm for 1 min. The RNA of SARS-CoV-2 was bound and released on Na^+-SC or Gu^+-SC column then its sample was amplified under three RT-PCR detection signals; FAM (SARS-CoV-2 Virus RNA fluorescence signal), VIC (human host cell RNA fluorescence signal), and Cy5 (Mastermix fluorescence signal as a control). in the amplification kit). Commercial extraction columns from QIAGEN® were also included in this method as a control column.

3. RESULTS AND DISCUSSION

3.1 Preparation of Kaolinite-Based SC and Its Derivatives with Chaotropic Ions

The raw kaolinite must initially go through pre-treatment methods which consist of three purification steps, to remove impurities on its amorphous layer. The activated raw kaolinite then went through the first purification steps with sodium acetate buffer solutions adjusted to pH 5. This purification process must be maintained at pH 5 to release carbonate salts to CO_2 (Ming and Dixon, 1987; Shackelford et al., 1997). The next purification step is the dispersion of the kaolinite into 30% H_2O_2 solutions aimed to remove natural organic matter that is still left in the layer or faces. As oxidizing agents, H_2O_2 would decrease organic matter by a peroxidic-type reaction without O_2 formations (Mikutta et al., 2005; Watts et al., 2002). Furthermore, several aromatic organic compounds may be removed by H_2O_2 as well, for example, phenolic compounds adsorbed to clay were oxidized directly, while those containing groups tended not to be reactive towards H_2O_2 (Andreozzi et al., 2002). The series of kaolinite purification steps ended with the dispersion into a sodium citrate-dithionite-bicarbonate to allow the dissolution of iron oxides from kaolinite faces (Eusterhues et al., 2003; Sokolova et al., 2017). The purified kaolinite was then activated to metakaolin by the calcination with overall reactions, expressed by equations below:

$$\underset{\text{Kaolinite}}{Al_2O_3.2SiO_2.2H_2O} \rightarrow \underset{\text{Metakaolin}}{Al_2O_3.2SiO_2(s)} + \underset{\text{Water}}{H_2O(g)}$$

During the calcination treatment, as shown by the reaction above, the dihydroxylation of H_2O interstitials molecule inside its interlayer will have occurred and decreased strength of aluminosilicate bond from kaolinite framework (Tironi et al., 2012). Thus, metakaolin will provide more reactive silica and alumina so that Si–O–Al bond could be cleaved upon the extraction process with aquaregia solutions in reflux apparatus (Cheng et al., 2021; Valeev et al., 2021). Based on the XRF measurement, all of these pre-treatment and extraction process carried on this work has successfully increased 91-92% SiO_2 content.

Subsequently, the extraction process formed metakaolin with net negative charged-basal and edge faces due to decreased Al^{3+} and other impurities ions at low pH conditions. Kaolinite tends to have negative sites on the basal faces and amphoteric sides on the edge face (Gupta and Miller, 2010; Kretzschmar et al., 1997; Chen et al., 2017). These amphoteric sites could either be negative or positively charged depending on the sys-

tem's pH. Meanwhile, the basal faces of kaolinite carried negative charges owing to the substitutions of the central Al^{3+} ions on the alumina octahedral layer with lower positive valence ions (He et al., 2011; Zhang et al., 2018). However, several studies showed that octahedral sheet in the basal faces also has amphoteric tendencies (Tombácz and Szekeres, 2006; Hong et al., 2007).

The overall negative sites on the basal and edge faces were balanced by chaotropic cations from the subsequent treatment of SC by dispersion into CH_3COONa 2 M or GuSCN 5 M solutions. In this work, the chaotropic cations Na^+ and Gu^+ have dual roles; as substituted ions inside lattice vacancies of metakaolin-based SC and modify their faces for obtained SC derivatives which tend to be net positively charged and expected to bind with PO_4^{3-} groups from RNA of SARS-CoV-2 nucleotide.

3.2 Characterizations of SC and Its Derivatives with Chaotropic Ions (Na^+ and Gu^+)

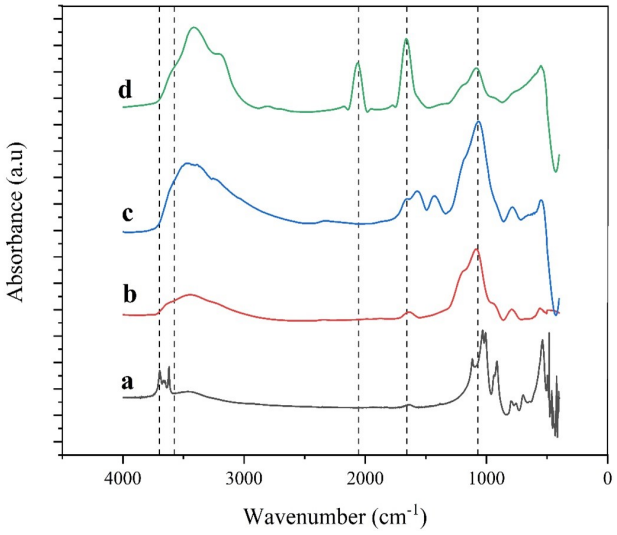

Figure 1. FTIR Spectra of a. Raw Kaolinite, b. SC, c. Na^+-SC, and d. Gu^+-SC

Figure 1 shows FTIR spectra of Indonesian raw kaolinite (a), metakaolin-based Silica Coarse (SC) (b), Na^+-SC (c), and Gu^+-SC (d). It shows that initially Indonesian raw kaolinite has two sharp peaks between 3700 cm^{-1} and 3614 cm^{-1} which are assigned to the stretching vibration of hydroxyl groups that belong to the structural, Si−OH and Al−OH, respectively, which is a typical character of natural phyllosilicate aluminosilicates. Furthermore, there is an observed peak identified as H−O−H bending vibrations at 1636 cm^{-1} which indicates the presence of water molecules in the interlayer space in the kaolinite framework (Stylianou et al., 2018). A broad peak in the range of 1117 cm^{-1} -1004 cm^{-1} was identified as Si–O–Si asymmetric stretching vibrations and 535 cm^{-1} was identified as Si–O–Al stretching vibrations.

After calcination treatment to form metakaolin, the two sharp peaks attributed to ~Si−OH and ~Al−OH merged into one broadband at 3700 cm^{-1}-3500 cm^{-1}; as shown in SC, Na^+-SC and Gu^+-SC in Figure 1. Furthermore, a peak at 535 cm^{-1} which was initially attributed to Si–O–Al groups disappeared, indicating the successful pre-treatment or purification methods for the raw kaolinite (Krisnandietal·,2019) . At the same time, there is a strong peak at 1066 cm^{-1}-1022 cm^{-1} which was identified as asymmetric stretching vibration of Si–O–Si; as seen on curve b, c, and d. Also, on the FTIR spectra of Gu^+-SC, there are high and sharp peaks at 2058 cm^{-1} which are identified as stretching vibrations S–C–N and at 1660 cm^{-1} which are identified as stretching vibrations C=N. The appearance of the two absorption peaks attributed to thiocyanate bonds was evidence of the existence of GuSCN.

The XRD pattern of raw kaolinite is shown in Figure 2, while the XRD pattern of all kaolinite-based SC and its derivatives were shown in Figure 3. The XRD pattern of raw kaolinite minerals before any treatment is represented in Figure 2. The majority of the mineral phases in kaolinite are aluminosilicate kaolinite (K) and halloysite (H) phases; while the second phase consists of silica quartz phase (α-quartz, Q), dickite phase (D), some Fe oxide compounds, and other impurities (Sagapoa et al., 2011; Senoussi et al., 2016). The typical peaks of mineral kaolinite (K) are found at 12.31°; 21.65°; 24.61°; 26.86°; 35.06° and 38.58°.

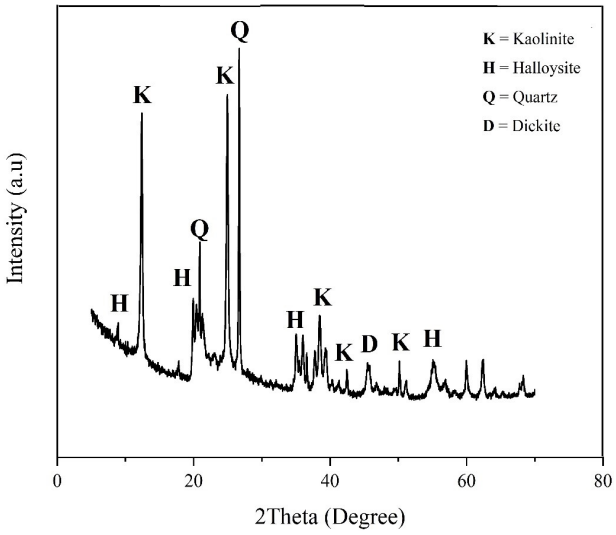

Figure 2. XRD Patterns of Mineral Phases Present in Raw Kaolinite

The experimental kaolinite-based Silica Coarse (SC) is represented by Figure 3b, which is modified to its derivatives in the form of Na^+-SC (Figure 3c) and Gu^+-SC (Figure 3d). These experimental spectra correlate well with the simulated theoretical diffraction of silica quartz from a published crystal structure (SiO_2 Quartz, JCPDS 00-046-1045, Figure 3a). The inset figure in Figure 3a visualizes the crystal structure of SiO_2 quartz from metakaolin extraction through a ball and stick model of the cubic cell. The expected pattern of SiO_2 quartz from

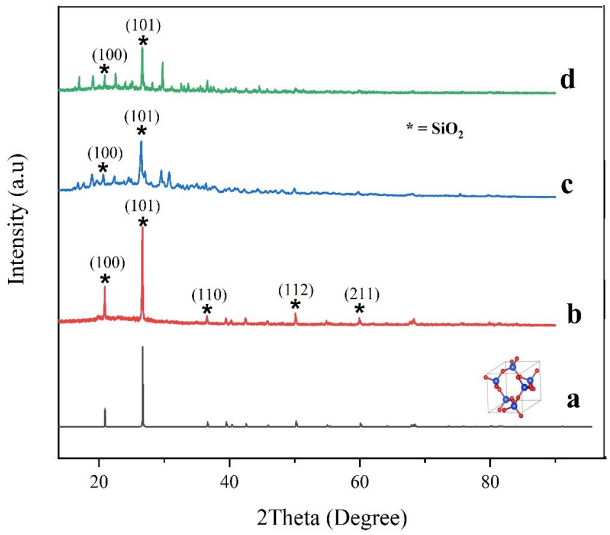

Figure 3. XRD Patterns of a. Theoretical XRD Pattern of SiO_2 Quartz Simulated by VESTA Based on JCPDS 00-04601045 and Experimental XRD Patterns of b. Kaolinite-Based SC, c. Na^+-SC, and d. Gu^+-SC

kaolinite was obtained at 20.96°, 26.69°, 36.63°, 50.23°, and 60.11°. The peaks assigned to the α-quartz phase with specific indexes (100), (101), (110), (112), and (211) happened because of the calcination and extraction process (Daou et al., 2020; Oyebanjo et al., 2020). Another sodium-containing species was also found at Na^+-SC (Figure 3c), at 18.78°; 29.61°; 30.78° (Iftitahiyah et al., 2018). The pattern is also in agreement with the calculated XRD from other kaolinite-based silica quartz (Tironi et al., 2012). As seen in Figure 3, the degree of crystallinity from SC derivatives decreases along with the addition of highly concentrated chaotropic agents. Also, some additional peaks in the Na^+-SC and Gu^+-SC patterns indicate the presence of crystalline impurities. This means that the presence of chaotropic ions can affect SC faces and be nonnegligible (Rahman et al., 2018).

Morphology from all modified kaolinite-based SC was examined by SEM. The SEM images of SC (Figure 4a.), display an irregular layer structure resulting from the aluminosilicate's collapsed amorphous structure after a series of pre-treatment to the layered kaolinite (Margenot et al., 2016). Meanwhile; SEM images of Na^+-SC (Figure 4b.) had a morphology with few holes on the surfaces which indicates that CH_3COONa addition can affect its surfaces (Fujiwara et al., 2011; Shi et al., 2013). More detail on SEM images of Gu^+-SC (Figure 4c) shows that the morphology of this modified coarse possessed rough surfaces and a few sharp-edged particles. This morphology structure indicates GuSCN as organic compounds have already deposited under the SiO_2 surfaces (Kröger et al., 2000; Selk et al., 2008).

BET and BJH methods of nitrogen desorption were taken into account to determine the specific surface area and pore characteristics of modified SC volumetrically (Djubaedah et al., 2020). As observed in all of the isotherm curves (Figure 5a) are classified as Type IV isotherms. Especially with the appearance of a hysteresis loop, the main pore structure of Indonesian kaolinite-based SC is mesopores. According to Thommes et al. (2015) the hysteresis loop that is shaped on Na^+-SC and Gu^+-SC is classified as the H4 hysteresis loop type which is often found in aggregated crystals of zeolites, some mesoporous zeolites, and micro-mesoporous materials. This means that some of the micropores networks are filled so that both modified SC surfaces are dominated by larger pores. This came in agreement with their pore size diameter (Figure 5b), in which Na^+-SC has the highest peak at 4.82 nm and Gu^+-SC BJH distribution pore curve has the highest peak at 4.30 nm. A summary of the surface area and pore size analysis data for the entire modified kaolinite-based SC is shown in Table 1. These results also could be considered to be the factors that supported the release of RNA from SARS-CoV-2 happened in the extraction method.

3.3 RNA Extraction Method of SARS-CoV-2 with Na^+-SC and Gu^+-SC Column

The RNA extraction method of SARS-CoV-2 started with suspension columns or wet pellet first, aimed to validate the proper formula of SC derivatives so that it could be further implemented in the form of powders (dry pellet). The relative concentration of SARS-CoV-2 RNA was measured with UV-Vis Nanodrop2000 Spectrometer before and after the treatment, the obtained results are in Supplementary Materials, Table 2. The relative purity of nucleic acids on the UV-Vis Nanodrop2000 Spectrometer is indicated by the ratio A_{260}/A_{280} and A_{260}/A_{230}. The wavelength of 260 nm (A_{260}) is the concentration of nucleic acids and 280 nm (A_{280}) is the protein contaminant in the sample. Besides, the absorptions wavelength of A_{230} is a wavelength range that can identify the presence of some other chemical contaminants (Shen, 2019).

The principle of the extraction method is to carry out the binding and releasing of nucleic acids (Esser et al., 2006; Tan and Yiap, 2009). The released RNA samples were then analyzed by RT-PCR test, to detect and quantify the fluorescence signal generated from each PCR cycle (Delidow et al., 1993). All samples of SARS-CoV-2 RNA used in this study have Ct value of < 20, this depends on lower Ct values are associated with a higher probability of positive SARS-CoV-2 viral culture (Phillips et al., 2022). Ct value could be considered as the proportional value to the number of nucleic acids on the PCR cycle (Prada Arismendy and Castellanos, 2011). The results showed that the extraction method with the suspension column succeeded in giving a sample that could be detected under the RT-PCR fluorescence signal. Due to the success of RNA samples from SC suspension column which could be detected under RT-PCR, this work also determined the reproducibility of all modified SC columns through the distributions of scattered dots within the grouped column (Figure 6). This aimed to evaluate the accuracy and precision between Na^+-SC and Gu^+-SC suspension or wet pellet columns, referring to several

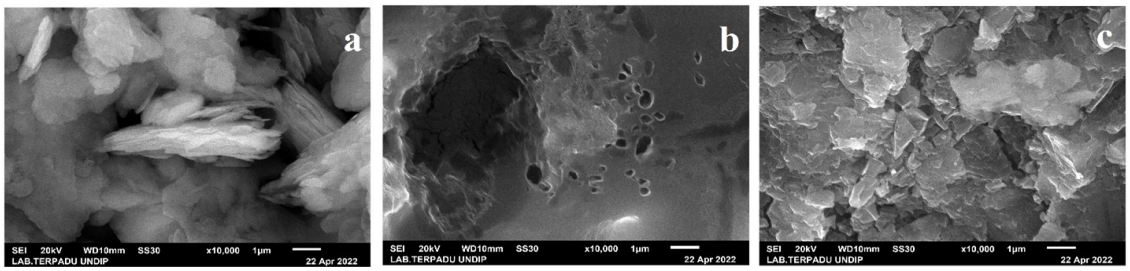

Figure 4. SEM Images of a. SC, b. Na^+-SC, and c. Gu^+-SC

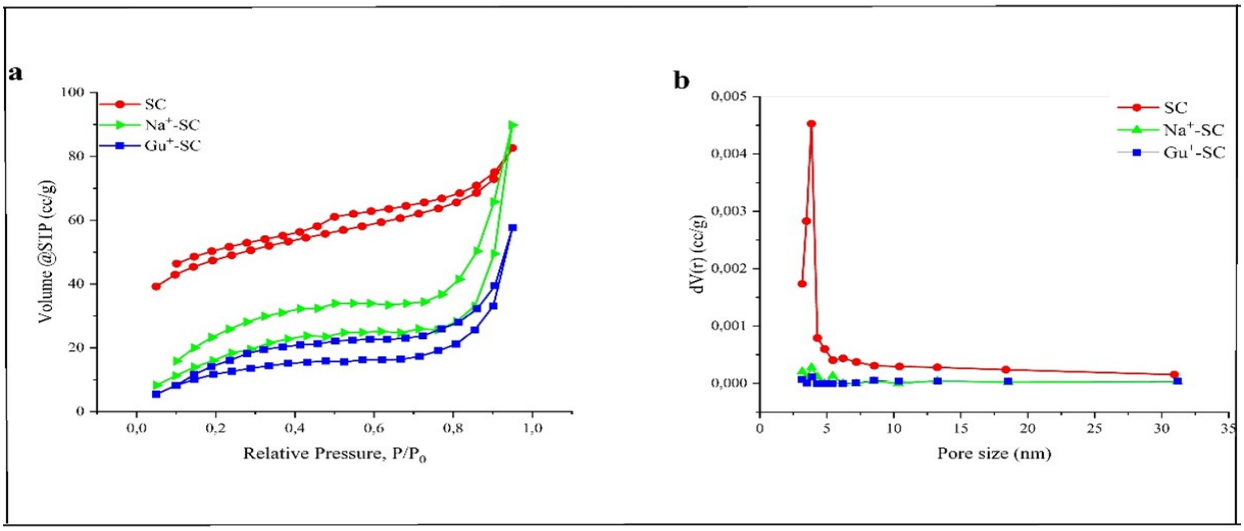

Figure 5. a. N_2 Adsorption-Desorption Isotherms Curve and b. Pore Size Distribution Curve of SC and Its Derivatives

studies that related to this research (Wu et al., 2018). The quality of measurement of separation methods and chromatography in the health sector must refer to accuracy and precision (Betz et al., 2011). Accuracy is a measure of the closeness of the experimental value to the actual value from the substance in the matrix, which in this work is the closeness of the final Ct Value after the extraction method with initial Ct Value. While precision is a measurement of the proximity of experimental results to each other, which in this work is determined with SD value and the distribution of scattered dots in the grouped column. Table 2 summarizes the mean and SD Data from initial and final Ct values from RNA samples released by SC-derivatives column and QIAGEN. From Figure 6, the reproducibility also can be represented with resulting stacked scattered dots, not far apart within its grouped columns.

On the other hand, the overall results of the extraction method with dry pellet almost entirely gave a negative response under RT-PCR fluorescence signals or were not detected. Considering the results with powder column tend to be not detected under RT-PCR device, other indicators are needed to prove the binding ability of powders to RNA of SARS-CoV-2. Another indicator is the measurement and analysis of the entire dry pellet after being used in extraction measurement by analysis with FTIR-ATR (Attenuated Total Reflectance)

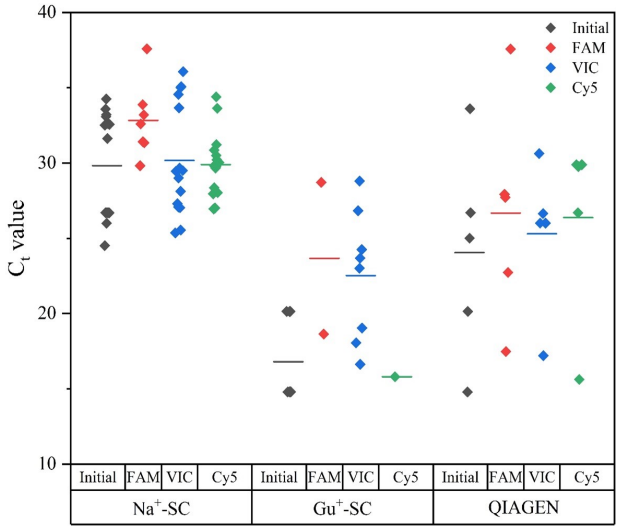

Figure 6. Grouped Scattered-Dot Column From Initial and Final Ct Value of SARS-CoV-2 RNA

instrument (Dovbeshko et al., 2000; Kelly et al., 2011). This spectroscopy technique was used to identify if there was any part of SARS-CoV-2 RNA which bounded to the Na^+-SC and

Table 1. Summary of Surface Area and Pore Volume Distribution of Indonesian Kaolinite-Based SC and Its Derivatives with Chaotropic Agents

Materials	SBET (m^2/g)	Smeso (m^2/g)	Vtotal (cc/g)	Vmeso (cc/g)	*d* Pore Size (nm)
SC	154	92	0.13	0.095	3.86
Na+-SC	70	49	0.0040	0.74	4.82
Gu+-SC	48	41	0.0040	0.73	4.30

Table 2. Mean and Standard Deviation (SD) data from Initial and Final Ct Value of RT-PCR Using Variances of Extraction Column

Extraction Columns	Initial Ct Value of RT-PCR (FAM)	Final Ct Value of RT-PCR		
		FAM	VIC	Cy5
Na^+-SC	30.97 ± 3.46	32.84 ± 2.49	30.17 ± 3.71	29.89 ± 2.14
Gu^+-SC	17.47 ± 3.78	23.69 ± 7.13	22.53 ± 4.30	15.8 ± 0.00
QIAGEN spin-column (Control)	24.05 ± 7.08	26.68 ± 7.44	25.30 ± 4.92	26.37 ± 6.16

Table 3. The Calculated peak area of PO_4^{3-} Vibrations ATR Spectra from Powder Extraction Columns (Calculated by peak analyzer feature from ORIGIN Software)

Extraction Columns (in the Form of Powder)	Mean ± Standard Deviation (SD) of Calculated Peak Area
Na^+-SC	20.43 ± 8.95
Gu^+-SC	23.10 ± 12.27

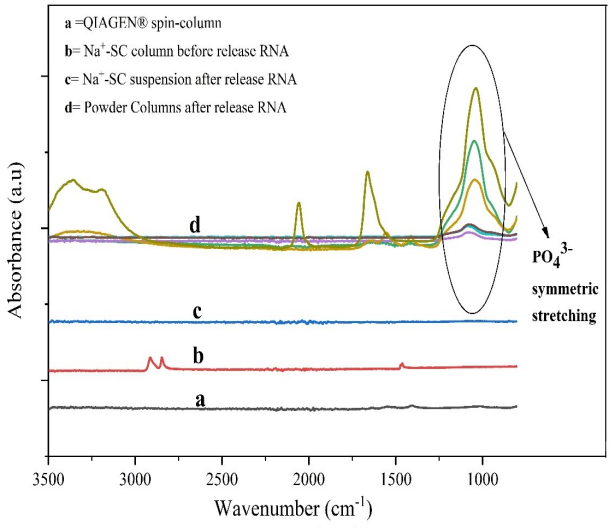

Figure 7. FTIR ATR Spectra of a. QIAGEN Spin-Column and, b. Na^+-SC Column Before Used for RNA Extraction Method Compared to c. Na^+-SC Suspension and d. Powder Column After Used for the RNA Extraction Method.

Gu^+-SC dried pellet, through the certain peaks that appear on FTIR ATR spectra. From the spectra shown in Figure 7, the SC-derivatives in the form of powder column were proven

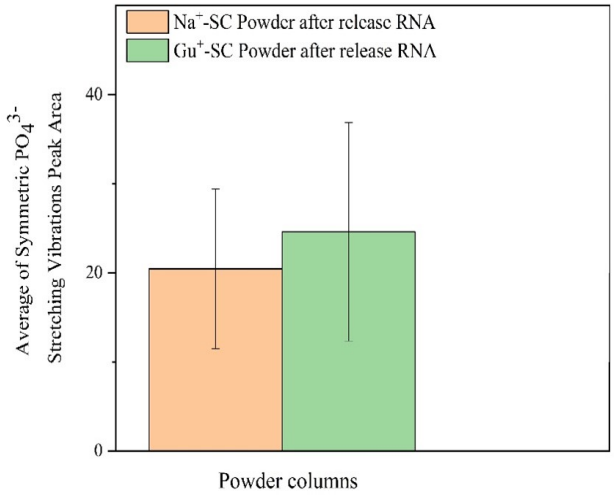

Figure 8. PO_4^{3-} Peak Area Analysis from FTIR ATR Measurement Through Na^+-SC and Gu^+-SC Powder After SARS-CoV-2 RNA Released

to be able to bind the RNA of SARS-CoV-2, but it requires further optimization to release the nucleic acids to collection tube. In Figure 7 a-c, no peak appeared, but there is a strong peak at 1050 cm^{-1} on ATR spectra of SC derivatives powder (Figure 7d) This peak was identified as a symmetric stretching vibration of PO_4^{3-} from the nucleobases of the SARS-CoV-2 virus.

Referring to the semi-quantification study of the relationship between the peak area from the FTIR ATR analysis and the affinities on the certain materials-based surface (Comeau and Willett, 2018), the calculation of the average peak area from the PO_4^{3-} vibrations in ATR measurements could be employed to estimate how much RNA is bound to powders column. The calculation of the normalized peak area and its average is available in Table 3 and its diagram is displayed in

Table 4. Ct Value from SARS-CoV-2 RNA Extracted by Powder Extraction Columns

Powder Extraction Column	Initial Ct Value of RT-PCR (FAM)	Final Ct Value of RT-PCR, After Extracted by Powder Extraction Columns		
		FAM	VIC	Cy5
Na^+-SC	18.81	-	-	-
QIAGEN (Control)		20.97	20.78	16.59
Gu^+-SC	14.14	28.68	18.75	-
QIAGEN (Control)		16.73	16.81	15.36

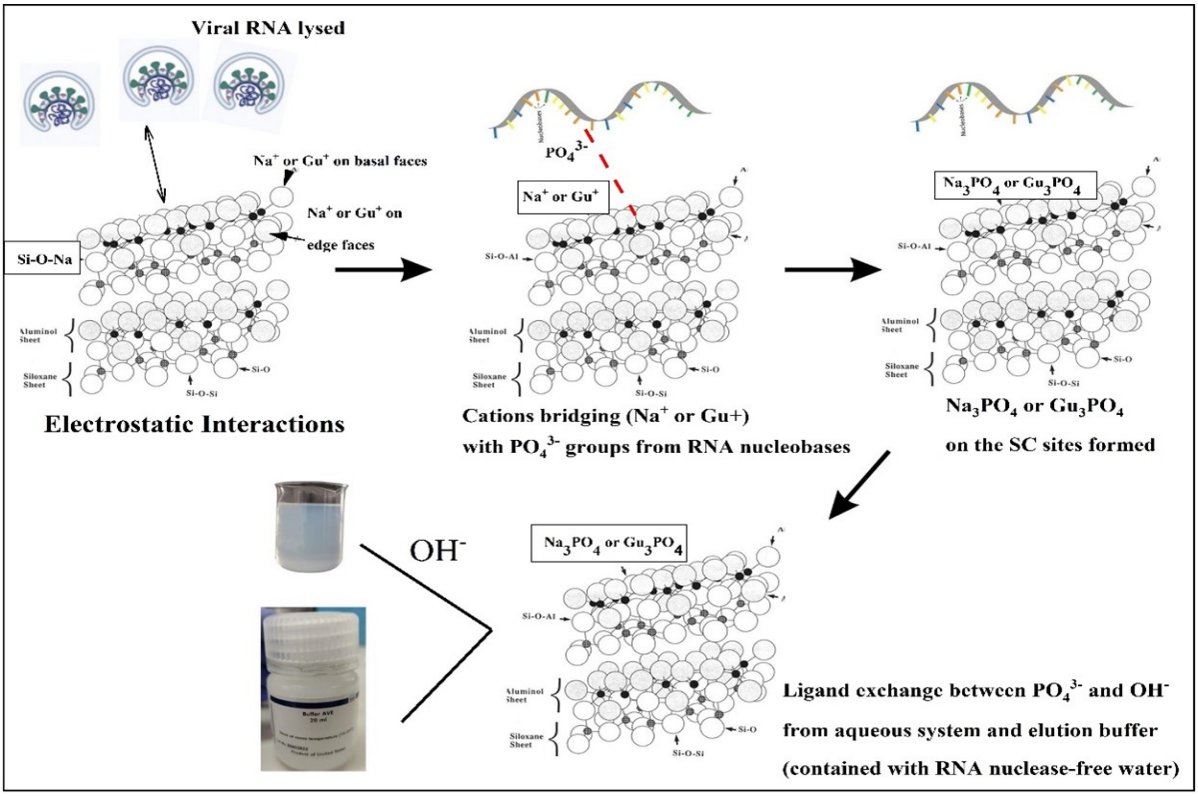

Figure 9. Scheme of Proposed Mechanism between RNA of SARS-CoV-2 with Modified-SC Suspension Column or Wet Pellets

Figure 8. The calculation also reveals that Gu^+-SC powder gave a larger peak area than Na^+-SC, indicative of the capability to bind more nucleic acids. The results were in accordance with the final Ct value from the RT-PCR test (Table 4). There is one column of Gu^+-SC powder that is capable of providing a detectable sample under FAM and VIC signals. These results are in agreement with the Hofmeister Series theory; that GuSCN is a strong chaotropic agent capable of rapidly inactivating RNAse enzyme inhibitors. The high molarity of GuSCN solutions used in the Gu^+-SC preparation also reduced endogenous RNAse activities that otherwise degrade cellular RNA components (Fuchs et al., 2017; Kunz et al., 2004; Pegram et al., 2010).

From the results gathered and analyzed in this work, a schematic mechanism of binding and releasing RNA of SARS-CoV-2 is proposed (Figure 9). This mechanism could explain the reasons behind the feasibility of RNA released from a suspension column rather than from the powder one. The basic concept of nucleic acid adsorptions on minerals includes three mechanisms: electrostatic interactions, formation of cationic bridges, and ligand exchange (Franchi and Gallori, 2004). Referring to these concepts, it can be related that the first mechanism from this work is in the form of electrostatic interaction between chaotropic ions and phosphate groups of the SARS-CoV-2 RNA. The second mechanism is RNA and chaotropic ions on the basal and edge faces will associate through the formation of cations bridging. Nucleic acid adsorptions will be increased along with the high concentrations of cations in the solution (Lorenz and Wackernagel, 1987). This is one of the reasons for using CH_3COONa and GuSCN solutions which have a fairly high molar concentration, 2 M and 5 M respectively.

This mechanism is terminated with ligand exchange between the phosphate (PO_4^{3-}) groups of the RNA and the hydroxyl (OH^-) group derived from the aqueous system of the suspension column. A related study (Hou et al., 2014) described that ligand exchange can be one of the important considerations in facilitating the release of nucleic acids from raw mineral-based surfaces. The exchange between OH-groups and PO_4^{3-} groups helps SARS-CoV-2 RNA be released so that it can be further analyzed in the RT-PCR molecular test. The mechanism for the adsorption of SARS-CoV-2 RNA on the surface of a suspension column or wet pellet is illustrated in the Figure 9.

4. CONCLUSIONS

A series of work that has been carried out, both including characterizations and RNA of SARS-CoV-2 extraction method, showed that the modified Silica Coarse (SC) based on the Indonesian raw kaolinite was successfully prepared and could be implemented in extraction methods of RNA SARS-CoV-2. From the results of RT-PCR analysis, the Na^+-SC and Gu^+-SC in the form of a suspension column have succeeded in providing results that can be detected under three RT-PCR fluorescence detection signals; FAM, VIC, and Cy5. Meanwhile, only the Gu^+-SC powder matrix can be detected under the RT-PCR in the powder column. To conclude, all SC derivatives columns have proven to successfully bind the RNA of the SARS-CoV-2 virus. However, it requires further optimization to release the RNA from the powder column to be detected under amplification techniques on an RT-PCR device.

5. ACKNOWLEDGMENT

This work received funding grant from KEMENRISTEK-BRIN and the Indonesia Endowment Funds for Education (LPDP) with Project No. 33/FI/P-KCOVID-19.2B3/IX/2020. Irena Khatrin, M.Si was appreciated for her data analysis assistance.

REFERENCES

Abdullah, I., W. Wibowo, S. Kosela, and Y. K. Krisnandi (2020). The Use of Silica Extracted from Kaolin as Catalyst Support for Esterification of 4-Hydroxybenzoic Acid with Sucrose. *Jurnal Kimia Sains dan Aplikasi*, **23**(6); 196–202

Ali, N., R. d. C. P. Rampazzo, A. D. T. Costa, and M. A. Krieger (2017). Current Nucleic Acid Extraction Methods and Their Implications to Point-Of-Care Diagnostics. *Biomed Research International*, **2017**; 1–13

Andreozzi, R., A. D'Apuzzo, and R. Marotta (2002). Oxidation of Aromatic Substrates in Water/goethite Slurry by Means of Hydrogen Peroxide. *Water Research*, **36**(19); 4691–4698

Baham, J. and G. Sposito (1994). Adsorption of Dissolved Organic Carbon Extracted from Sewage Sludge on Montmorillonite and Kaolinite in the Presence of Metal Ions. 23 1, Wiley Online Library, 147–153

Betz, J. M., P. N. Brown, and M. C. Roman (2011). Accuracy, Precision, and Reliability of Chemical Measurements in Natural Products Research. *Fitoterapia*, **82**(1); 44–52

Boom, R., C. Sol, M. Salimans, C. Jansen, P. Wertheim-van Dillen, and J. Van der Noordaa (1990). Rapid and Simple Method for Purification of Nucleic Acids. *Journal of Clinical Microbiology*, **28**(3); 495–503

Chen, H., L. K. Koopal, J. Xiong, M. Avena, and W. Tan (2017). Mechanisms of Soil Humic Acid Adsorption onto Montmorillonite and Kaolinite. *Journal of Colloid and Interface Science*, **504**; 457–467

Cheng, H., Y. Huang, Z. Zhu, L. Dong, J. Zha, and M. Yu (2021). Enhanced $PbCl_2$ Adsorption Capacity of Modified Kaolin in the Furnace Using a Combined Method of Thermal Pre-Activation and Acid Impregnation. *Chemical Engineering Journal*, **414**; 128672

Comeau, P. and T. Willett (2018). Impact of Side Chain Polarity on Non-Stoichiometric Nano-Hydroxyapatite Surface Functionalization with Amino Acids. *Scientific Reports*, **8**(1); 12700

Daou, I., G. L. Lecomte Nana, N. Tessier Doyen, C. Peyratout, M. F. Gonon, and R. Guinebretiere (2020). Probing the Dehydroxylation of Kaolinite and Halloysite by in Situ High Temperature X-Ray Diffraction. *Minerals*, **10**(5); 480

Delidow, B. C., J. P. Lynch, J. J. Peluso, and B. A. White (1993). Polymerase Chain Reaction: Basic Protocols. *PCR Protocols: Current Methods and Applications*; 1–29

Ding, J., X. Xu, Y. Deng, X. Zheng, and T. Zhang (2024). Comparison of RT-ddPCR and RT-qPCR Platforms for SARS-CoV-2 Detection: Implications for Future Outbreaks of Infectious Diseases. *Environment International*, **183**; 108438

Djubaedah, E., A. Wulandari, and K. Krisnandi (2020). Surface Area Modification of Natural Zeolite Through NaCl Counterbalanced Treatment to Apply in Adsorption Heat Storage System. *Evergreen*, **7**(1); 26–31

Dovbeshko, G. I., N. Y. Gridina, E. B. Kruglova, and O. P. Pashchuk (2000). FTIR Spectroscopy Studies of Nucleic Acid Damage. *Talanta*, **53**(1); 233–246

Esser, K. H., W. H. Marx, and T. Lisowsky (2006). Maxxbond: First Regeneration System for DNA Binding Silica Matrices. *Nature Methods*, **3**(1); i–ii

Eusterhues, K., C. Rumpel, M. Kleber, and I. Kögel-Knabner (2003). Stabilisation of Soil Organic Matter by Interactions with Minerals As Revealed by Mineral Dissolution and Oxidative Degradation. *Organic Geochemistry*, **34**(12); 1591–1600

Farkas, D. H. and C. A. Holland (2009). Overview of Molecular Diagnostic Techniques and Instrumentation. In *Cell and Tissue Based Molecular Pathology*. Elsevier, pages 19–32

Franchi, M. and E. Gallori (2004). Origin, Persistence and Biological Activity of Genetic Material in Prebiotic Habitats. *Origins of Life and Evolution of the Biosphere*, **34**; 133–141

Frost, R. L., J. Kristof, L. Rintoul, and J. T. Kloprogge (2000). Raman Spectroscopy of Urea and Urea-Intercalated Kaolin-

ites at 77 K. *Spectrochimica Acta Part A: Molecular and Biomolecular Spectroscopy*, **56**(9); 1681–1691

Fuchs, T. C., G. L. Truisi, and P. G. Hewitt (2017). Toxicogenomics in Preclinical Development. In *A Comprehensive Guide to Toxicology in Nonclinical Drug Development*. Elsevier, pages 893–920

Fujiwara, M., K. Shiokawa, M. Araki, M. Nakao, I. Sakakura, and Y. Nakahara (2011). Preparation of Silica Thin Films with Macropore Holes from Sodium Silicate and Polymethacrylate: An Approach to Formation Mechanism of Diatomaceous Earth like Silica Hollow Particles. *Chemical Engineering Journal*, **172**(2-3); 1103–1110

Gibson, N. J. (2006). The Use of Real-Time PCR Methods in DNA Sequence Variation Analysis. *Clinica Chimica Acta*, **363**(1-2); 32–47

Gunawan, Y., N. Putra, E. Kusrini, I. I. Hakim, and M. D. H. Setiawan (2020). Study of Heat Pipe Utilizing Low-Temperature Geothermal Energy and Zeolite-A for Tea Leaves Withering Process. *Evergreen*, **7**(2); 221–227

Gupta, V. and J. D. Miller (2010). Surface Force Measurements at the Basal Planes of Ordered Kaolinite Particles. *Journal of Colloid and Interface Science*, **344**(2); 362–371

He, M. C., J. Zhao, Z. J. Fang, and P. Zhang (2011). First-Principles Study of Isomorphic ('Dual-Defect') Substitution in Kaolinite. *Clays and Clay Minerals*, **59**(5); 501–506

Hong, H., X. Min, and Y. Zhou (2007). Orbital Calculations of Kaolinite Surface: On Substitution of Al^{3+} for Si^{4+} in the Tetrahedral Sites. *Journal of Wuhan University of Technology-Materials Science Edition.*, **22**(4); 661–666

Hou, Y., P. Wu, and N. Zhu (2014). The Protective Effect of Clay Minerals against Damage to Adsorbed DNA Induced by Cadmium and Mercury. *Chemosphere*, **95**; 206–212

Huang, Q., L. Zheng, Y. Zhu, J. Zhang, H. Wen, J. Huang, J. Niu, X. Zhao, and Q. Li (2011). Multicolor Combinatorial Probe Coding for Real-Time PCR. *PloS one*, **6**(1); e16033

Iftitahiyah, V. N., D. Prasetyoko, H. Nur, and H. Bahruji (2018). Synthesis and Characterization of Zeolite NaX from Bangka Belitung Kaolin As Alternative Precursor. *Malaysian Journal of Fundamental and Applied Sciences*, **14**(4); 414–418

Katevatis, C., A. Fan, and C. M. Klapperich (2017). Low Concentration DNA Extraction and Recovery Using a Silica Solid Phase. *PloS one*, **12**(5); e0176848

Kelly, J. G., J. Trevisan, A. D. Scott, P. L. Carmichael, H. M. Pollock, P. L. Martin-Hirsch, and F. L. Martin (2011). Biospectroscopy to Metabolically Profile Biomolecular Structure: A Multistage Approach Linking Computational Analysis with Biomarkers. *Journal of Proteome Research*, **10**(4); 1437–1448

Kretzschmar, R., H. Sticher, and D. Hesterberg (1997). Effects of Adsorbed Humic Acid on Surface Charge and Flocculation of Kaolinite. *Soil Science Society of America Journal*, **61**(1); 101–108

Kröger, N., R. Deutzmann, C. Bergsdorf, and M. Sumper (2000). Species-Specific Polyamines from Diatoms Control Silica Morphology. *Proceedings of the National Academy of Sciences*, **97**(26); 14133–14138

Kunz, W., P. L. Nostro, and B. W. Ninham (2004). The Present State of Affairs with Hofmeister Effects. *Current Opinion in Colloid & Interface Science*, **9**(1-2); 1–18

Ladha, A., J. Joung, O. O. Abudayyeh, J. S. Gootenberg, and F. Zhang (2020). A 5-min RNA Preparation Method for COVID-19 Detection with RT-qPCR. *MedRxiv*; 2020–05

Lau, S. K. and J. F. Chan (2015). Coronaviruses: Emerging and Re-Emerging Pathogens in Humans and Animals. *Virology Journal*, **12**(1); 1–3

Lee, H. R., T. Shibata, M. Kanezashi, T. Mizumo, J. Ohshita, and T. Tsuru (2011). Pore-Size-Controlled Silica Membranes with Disiloxane Alkoxides for Gas Separation. *Journal of Membrane Science*, **383**(1-2); 152–158

Loganathan, S., G. Pugazhenthi, S. Thomas, and T. Varghese (2017). An Overview of Polymer-Clay Nanocomposites. *Clay-Polymer Nanocomposites*, **2017**; 29–81

Lorenz, M. G. and W. Wackernagel (1987). Adsorption of DNA to Sand and Variable Degradation Rates of Adsorbed DNS. *Applied and Environmental Microbiology*, **53**(12); 2948–2952

Margenot, A. J., F. J. Calderón, K. W. Goyne, F. N. Dmukome, and S. Parikh (2016). Ir Spectroscopy, Soil Analysis Applications. In *Encyclopedia of Spectroscopy and Spectrometry*. Elsevier, pages 448–454

Mikutta, R., M. Kleber, K. Kaiser, and R. Jahn (2005). Organic Matter Removal from Soils Using Hydrogen Peroxide, Sodium Hypochlorite, and Disodium Peroxodisulfate. *Soil science society of America journal*, **69**(1); 120–135

Ming, D. W. and J. B. Dixon (1987). Technique for the Separation of Clinoptilolite from Soils. *Clays and Clay Minerals*, **35**; 469–472

Oyebanjo, O., G. I. Ekosse, and J. Odiyo (2020). Physico-Chemical, Mineralogical, and Chemical Characterisation of Cretaceous–Paleogene/neogene Kaolins within Eastern Dahomey and Niger Delta Basins from Nigeria: Possible Industrial Applications. *Minerals*, **10**(8); 670

Pegram, L. M., T. Wendorff, R. Erdmann, I. Shkel, D. Bellissimo, D. J. Felitsky, and M. T. Record Jr (2010). Why Hofmeister Effects of Many Salts Favor Protein Folding but Not DNA Helix Formation. *Proceedings of the National Academy of Sciences*, **107**(17); 7716–7721

Phillips, M. C., D. Quintero, N. Wald-Dickler, P. Holtom, and S. M. Butler-Wu (2022). SARS-CoV-2 Cycle Threshold (Ct) Values predict Future COVID-19 Cases. *Journal of Clinical Virology*, **150**; 105153

Prada Arismendy, J. and J. E. Castellanos (2011). PCR En Tiempo Real. Modelo De Aplicacion En Dengue. *Colombia Medica*, **42**(2); 243–259

Rahman, A. U., F. U. Khan, W. U. Rehman, and S. Saleem (2018). Synthesis and Characterization of Zeolite 4A Using Swat Kaolin. *Journal of Chemical Technology and Metallurgy*, **53**(5); 825–829

Rimola, A., D. Costa, M. Sodupe, J. F. Lambert, and P. Ugliengo (2013). Silica Surface Features and Their Role

in the Adsorption of Biomolecules: Computational Modeling and Experiments. *Chemical Reviews*, **113**(6); 4216–4313
Sagapoa, C. V., A. Imai, and K. Watanabe (2011). Laterization Process of Ultramafic Rocks in Siruka, Solomon Islands. *Kyushu University Global COE Program Journal of Novel Carbon Resource Sciences*, **3**; 32–39
Saragi, I. R., Y. K. Krisnandi, and R. Sihombing (2019). Synthesis and Characterization HY Zeolite from Natural Aluminosilicate for n-Hexadecane Cracking. *Materials Today: Proceedings*, **13**; 76–81
Selk, Y., T. Yoshida, and T. Oekermann (2008). Variation of the Morphology of Electrodeposited Copper Thiocyanate Films. *Thin Solid Films*, **516**(20); 7120–7124
Senoussi, H., H. Osmani, C. Courtois, and M. el Hadi Bourahli (2016). Mineralogical and Chemical Characterization of DD3 Kaolin from the East of Algeria. *boletín de la sociedad española de cerámica y vidrio*, **55**(3); 121–126
Shackelford, C. D., T. E. Cotten, K. M. Rohal, and S. H. Strauss (1997). Acid Buffering a High pH Soil for Zinc Diffusion. *Journal of geotechnical and geoenvironmental engineering*, **123**(3); 260–271
Shen, C. H. (2019). Detection and Analysis of Nucleic Acids. *Diagnostic Molecular Biology*; 167–185
Sheridan, C. (2020). Fast, Portable Tests Come Online to Curb Coronavirus Pandemic. *Nature biotechnology*, **38**(5); 515–518
Shi, J. Y., Y. Y. Wang, Q. Z. Yao, G. T. Zhou, and S. Q. Fu (2013). Bio-Inspired Synthesis of Silica Ribbons with Through-Holes. *Colloids and Surfaces A: Physicochemical and Engineering Aspects*, **436**; 664–674
Sokolova, T., I. Tolpeshta, Y. G. Izosimova, V. Umnova, and P. Lashukov (2017). The Effect of Treatment with Hydrogen Peroxide and the Mehra-Jackson Reagent on X-Ray Diffraction Patterns of Clay Fractions. *Eurasian Soil Science*, **50**; 1386–1394
Song, H. H., J. C. Choi, R. Lee, S. K. Yoon, H. J. Park, Y. H. Shin, J. W. Shin, and J. Kim (2024). Quality and Composition of Archived Nucleic Acids After Use in SARS-CoV-2 Molecular Testing. *Clinica Chimica Acta*, **554**; 117755
Stylianou, M., V. Inglezakis, A. Agapiou, G. Itskos, A. Jetybayeva, and M. Loizidou (2018). A Comparative Study on Phyllosilicate and Tectosilicate Mineral Structural Properties. *Desalination and Water Treatment*, **112**; 119–146
Tan, S. C. and B. C. Yiap (2009). DNA, RNA, and Protein Extraction: The Past and the Present. *BioMed Research International*, **2009**; 1–10
Teymouri, M., S. Mollazadeh, H. Mortazavi, Z. N. Ghale-Noie, V. Keyvani, F. Aghababaei, M. R. Hamblin, G. Abbaszadeh-Goudarzi, H. Pourghadamyari, and S. M. R. a. Hashemian (2021). Recent Advances and Challenges of RT-PCR Tests for the Diagnosis of Covid-19. *Pathology-Research and Practice*, **221**; 153443
Thommes, M., K. Kaneko, A. V. Neimark, J. P. Olivier, F. Rodriguez-Reinoso, J. Rouquerol, and K. S. Sing (2015). Physisorption of Gases, with Special Reference to the Evaluation of Surface Area and Pore Size Distribution (IUPAC Technical Report). *Pure and Applied Chemistry*, **87**(9-10); 1051–1069
Tironi, A., M. Trezza, E. Irassar, and A. Scian (2012). Thermal Treatment of Kaolin: Effect on the Pozzolanic Activity. *Procedia Materials Science*, **1**; 343–350
Tombácz, E. and M. Szekeres (2006). Surface Charge Heterogeneity of Kaolinite in Aqueous Suspension in Comparison with Montmorillonite. *Applied Clay Science*, **34**(1-4); 105–124
Toni, L. S., A. M. Garcia, D. A. Jeffrey, X. Jiang, B. L. Stauffer, S. D. Miyamoto, and C. C. Sucharov (2018). Optimization of Phenol-Chloroform RNA Extraction. *MethodsX*, **5**; 599–608
Valeev, D., D. Pankratov, A. Shoppert, A. Sokolov, A. Kasikov, A. Mikhailova, C. Salazar-Concha, and I. Rodionov (2021). Mechanism and Kinetics of Iron Extraction from High Silica Boehmite–Kaolinite Bauxite by Hydrochloric Acid Leaching. *Transactions of Nonferrous Metals Society of China*, **31**(10); 3128–3149
Valiant, W. G., J. Borman, K. Cai, and P. M. Vallone (2024). Efficient Extraction of Adventitious Virus Nucleic Acid Using Commercially Available Methods. *Biologicals*, **85**; 101741
Watts, R. J., P. C. Stanton, J. Howsawkeng, and A. L. Teel (2002). Mineralization of a Sorbed Polycyclic Aromatic Hydrocarbon in Two Soils Using Catalyzed Hydrogen Peroxide. *Water Research*, **36**(17); 4283–4292
Wicky, B. I., S. L. Shammas, and J. Clarke (2017). Affinity of IDPs to Their Targets Is Modulated by Ion-Specific Changes in Kinetics and Residual Structure. *Proceedings of the National Academy of Sciences*, **114**(37); 9882–9887
Wu, L., W. Wang, W. Zhang, H. Su, Q. Liu, J. Gu, T. Deng, and D. Zhang (2018). Highly Sensitive, Reproducible and Uniform SERS Substrates with a High Density of Three-Dimensionally Distributed Hotspots: Gyroid-Structured Au Periodic Metallic Materials. *NPG Asia Materials*, **10**(1); e462–e462
Yoo, B., M. G. Kim, A. Y. Min, D. W. Seo, S. H. Kim, and S. H. Kim (2023). Optimization of RT-PCR Methods for Enterovirus Detection in Groundwater. *Heliyon*, **9**(12); e23028
Zhang, N., A. V. Nguyen, and C. Zhou (2018). Impact of Interfacial Al and Si-Active Sites on the Electrokinetic Properties, Surfactant Adsorption and Floatability of Diaspore and Kaolinite Minerals. *Minerals Engineering*, **122**; 258–266
Zhang, Y. and P. S. Cremer (2006). Interactions between Macromolecules and Ions: The Hofmeister Series. *Current Opinion in Chemical Biology*, **10**(6); 658–663

